



HAL
open science

Comparison of Aero-Elastic Simulations and Measurements Performed on NENUPHAR's 600kW Vertical Axis Wind Turbine: Impact of the Aerodynamic Modelling Methods

F. Blondel, C. Galinos, U. Paulsen, P. Bozonnet, M. Cathelain, G. Ferrer, H.A. A Madsen, G. Pirrung, F. Silvert

► To cite this version:

F. Blondel, C. Galinos, U. Paulsen, P. Bozonnet, M. Cathelain, et al.. Comparison of Aero-Elastic Simulations and Measurements Performed on NENUPHAR's 600kW Vertical Axis Wind Turbine: Impact of the Aerodynamic Modelling Methods. *Journal of Physics: Conference Series*, 2018, 1037, pp.022010. 10.1088/1742-6596/1037/2/022010 . hal-01912171

HAL Id: hal-01912171

<https://ifp.hal.science/hal-01912171>

Submitted on 5 Nov 2018

HAL is a multi-disciplinary open access archive for the deposit and dissemination of scientific research documents, whether they are published or not. The documents may come from teaching and research institutions in France or abroad, or from public or private research centers.

L'archive ouverte pluridisciplinaire **HAL**, est destinée au dépôt et à la diffusion de documents scientifiques de niveau recherche, publiés ou non, émanant des établissements d'enseignement et de recherche français ou étrangers, des laboratoires publics ou privés.



Distributed under a Creative Commons Attribution 4.0 International License

PAPER • OPEN ACCESS

Comparison of Aero-Elastic Simulations and Measurements Performed on NENUPHAR's 600kW Vertical Axis Wind Turbine: Impact of the Aerodynamic Modelling Methods

To cite this article: F. Blondel *et al* 2018 *J. Phys.: Conf. Ser.* **1037** 022010

View the [article online](#) for updates and enhancements.

Comparison of Aero-Elastic Simulations and Measurements Performed on NENUPHAR's 600kW Vertical Axis Wind Turbine: Impact of the Aerodynamic Modelling Methods

F. Blondel¹, C. Galinos², U. Paulsen², P. Bozonnet¹, M. Cathelain¹, G. Ferrer¹, H.A. Madsen², G. Pirrung², F. Silvert³

¹ IFP Energies nouvelles, 1-4 avenue du Bois Préau, 92852 Rueil-Malmaison, France.

² Technical University of Denmark, DK 4000 Roskilde Denmark.

³ Nenuphar, 1 Rue du Professeur Calmette 59000 Lille, France.

E-mail: frederic.blondel@ifpen.fr

Abstract. Aero-elastic solver predictions are compared to measured data from the NENUPHAR's 1HS prototype, with a focus on the blade loads. Two solvers are investigated, namely the HAWC2 solver, and DeepLinesWindTM, respectively based on a linear and a non-linear formulation of the Timoshenko beam theory. Various aerodynamic models are used, from simple Multiple Streamtube models up to the Actuator-Cylinder flow model and 2D/3D Vortex flow solvers. A special attention is also given to the influence of the dynamic stall on the results. Aero-elastic solvers predictions are accurate and fit well with the measured blade loads, but this work emphasizes the fact that suitable aerodynamic model and stall model should be used.

1. Introduction

The aim of this paper is to present the work conducted within the EU INFLOW project on the simulation of NENUPHAR's straight-bladed, 600kW Vertical Axis Wind Turbine Prototype (see Pitance et al., [18] and Figure 1) using two aero-elastic simulation tools, namely HAWC2 (DTU) and DeepLines WindTM (PRINCIPIA/IFPEN). Simulation tool predictions will be compared

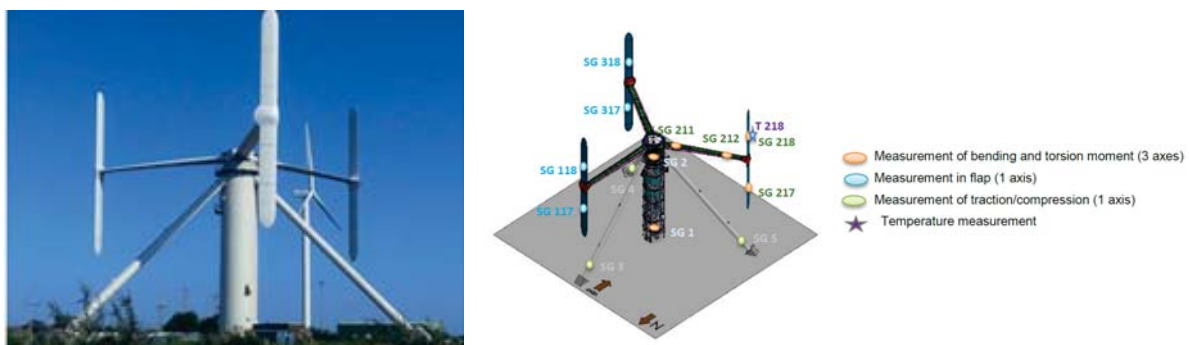


Figure 1. View of NENUPHAR's prototype (left) and Position of the strain gauges on the prototype (right).



with measurements from strain gages recorded during tests performed on the NENUPHAR's prototype. Strain gages measurements are performed on the upper and lower halves of the blades, as well as on the struts, near the root and near the blade attachment point, on the tower and its supporting structures as shown in Figure 1. Meteorological measurements are carried out on a 54 m meteorological mast located approximately at a distance of 200 m from the wind turbine. Wind velocities are measured at three different heights: 12.75, 27.3 and 54.1 meters, bending moment comparisons being performed at 21 and 33 meters in height, approximately. A power law coefficient is derived from these measurements. Based on this coefficient, hub-height mean wind velocity and turbulence intensity, wind files can be generated and used as inputs by the aero-elastic solvers. This paper will be organized as follows: first, focus is put on the aerodynamic modelling of vertical axis wind turbines. Then, simulation results obtained with the aero-elastic models will be compared to the measurements.

2. Aerodynamic models: description and comparison

2.1. Aerodynamic models: brief description

2.1.1. Multiple Streamtube Model (MSM). The MSM model belongs to the so-called "Blade Element Momentum" (BEM) methods. The wind turbine is divided into several adjacent streamtubes, and, similarly to the BEM model for horizontal wind turbines, an induction factor is computed for each streamtube: an equation system based on an expression for the thrust coefficient from actuator disk theory and another expression from blade element theory is solved for to obtain the induction factor. In the MSM model, no distinction is made between the upwind and the downwind part of the rotor.

2.1.2. 2D Vortex (V2D). In the V2D approach, the rotor is discretized into several sections, perpendicular to the main direction of the hub. In these sections, each blade element is represented by a point vortex (bound vortex). Each element has its own wake, wake elements (vortex points) being shed at each time step. During the convection steps, each wake element is influenced by the other wake and blade: the wake deforms freely. Blade forces are computed taking the induced velocities from the whole vortex system into account.

2.1.3. 3D Vortex (V3D). The V3D approach is an extension of the V2D model. In this model, the wind turbine blades are discretized using bound filaments (lifting-line approach), and the wake is discretized using both shed and trail filaments. Three-dimensional effects such as tip vortices are intrinsically accounted for, so that tip losses are taken into account. During the convection step, the influence of the whole vortex system on each vortex filament is taken into account, so that the wake deforms freely.

2.1.4. Actuator Cylinder (AC). The Actuator Cylinder flow model is an adaptation of the Actuator Disk model to VAWTs. The 2D version is used in this work, the rotor being discretized into several sections. In this model, reaction forces are applied on the flow as volume or body forces perpendicular and tangential to the rotor plane (see Madsen [13], Madsen et al. [14], Madsen et al. [15]).

2.1.5. Dynamic stall modelling. The four models used in the present study have to be corrected for dynamic stall effect, due to the "lifting-line" approach and the use of polar curves computed in steady conditions. IFPEN solvers (MSM, V2D, V3D) use the dynamic stall model of Øye, including modifications suggested by Blondel et al. [2]. These models will be denoted as Øye/MSM, Øye/V2D and Øye/V3D. Within the DTU solver (AC), a dynamic-stall model based on the work of Pirrung and Gaunaa [17], who proposed a modified version of the wind energy

adapted Beddoes-Leishman model [7], is used. When stall is activated, this model will be denoted as BL/AC.

2.2. Conventions

Before going through the results, it is important to define the conventions used in the rest of the paper. First of all, a convention is chosen for the azimuth angle (Figure 2). The wind blows from the left, in the direction of $\Phi = -90^\circ$. The VAWT rotates in the so-called counter-clockwise direction. Then, a convention is used for non-dimensioning the force in the aerodynamic models

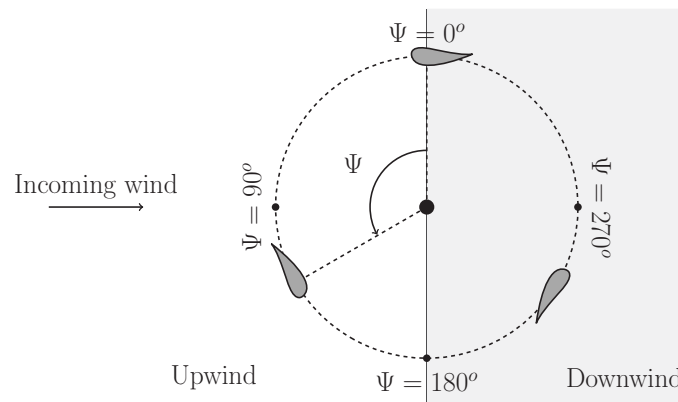


Figure 2. Convention used for the azimuth angle.

comparison. Both normal and tangential force coefficients are defined as follows:

$$C_{n,t} = \frac{F_{n,t}}{1/2\rho u_{eff}^2 c}, \quad (1)$$

where F_n and F_t are the normal and tangential forces (with respect to the chord), ρ is the fluid density, u_{eff} is the effective velocity (including induced velocities) and c is the chord of the considered profile. Conventions being defined, a comparison is drawn between various aerodynamic solvers. The geometry of NENUPHAR's wind turbine (Figure 3) prototype is used as a reference, but is considered as rigid.

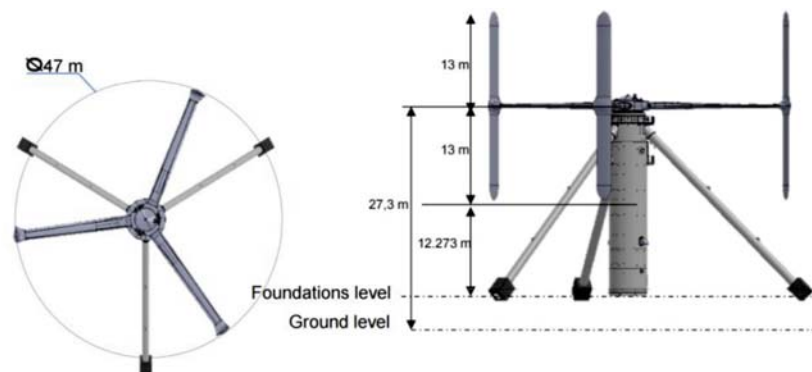


Figure 3. General dimensions of the 1HS prototype, from [19].

The airfoil polar data have been generated using the Stanford University Unstructured CFD solver (SU2), see Economou et al [5]. Even though no pure aerodynamic measurements (such as normal and tangential force) are available, this study will provide a basis to ensure the consistency between the predictions of each solver. Typical results are given in Figure 4 and Figure 5. Two Tip Speed Ratios (TSRs) are considered: a nominal one (around 3.85) and a lower one (around 1.92). In the second case, the attack angles are higher, and the flow is prone to dynamic stall. For the MSM, V2D and V3D simulations, 15 rotor rotations are performed, with a rotation of 5° per time step. For the AC model, a rotation of approximately 0.75° per time step is used.

2.3. High TSR, attached flow

At this high TSR, a very good agreement is obtained between vortex models and the AC model without dynamic stall (Figure 4, top). Differences occur in the downwind part, between azimuth 220° and 320° : a slight increase of the normal force and a decrease of the tangential force are observed with the AC flow model. Ferreira et al. [6] already observed these differences between

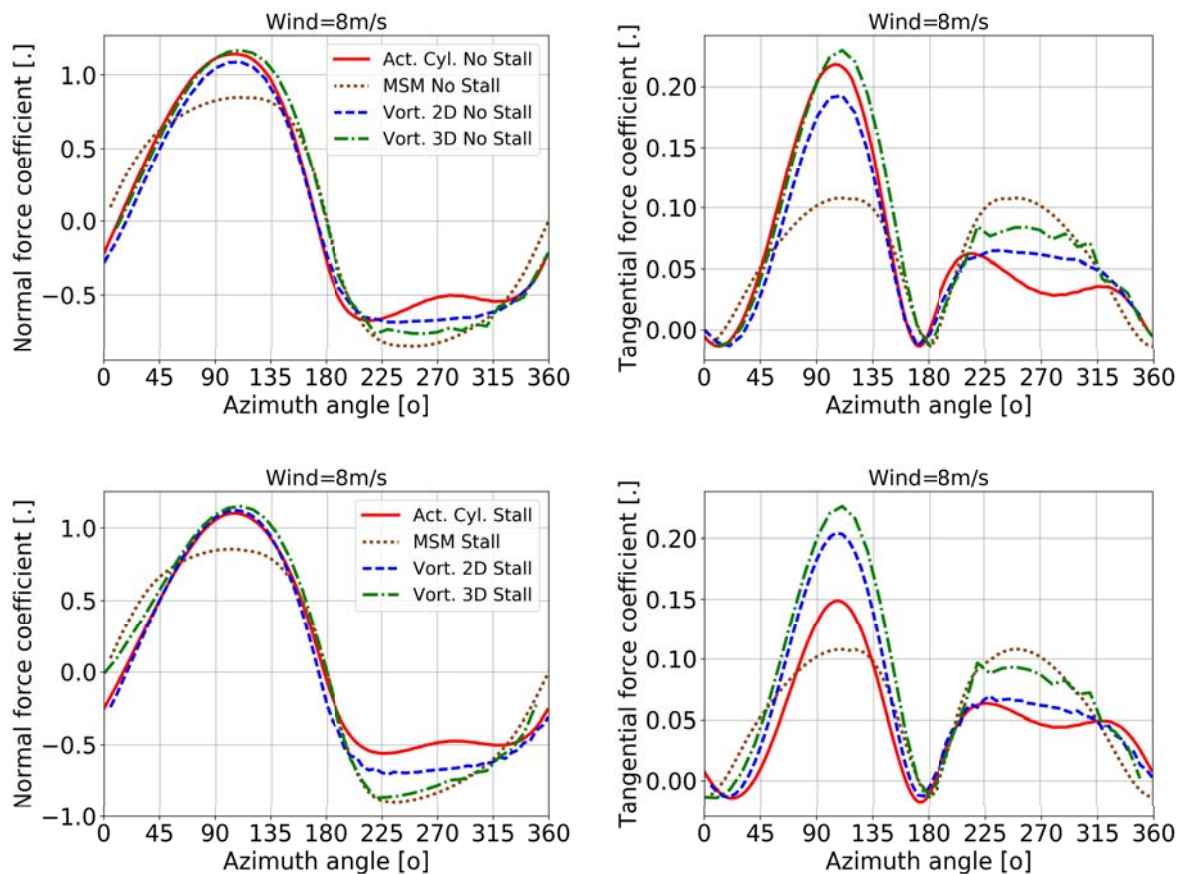


Figure 4. Normal (left) and tangential (right) force coefficients as a function of azimuthal position predicted by the AC model, the MSM model, the 2D and 3D vortex solvers without dynamic stall (top) and with dynamic stall (bottom) at $TSR=3.85$.

the AC and vortex methods, and attributed them to the use of a time averaged loading on the actuator. The MSM underestimates the normal and tangential force coefficients in the upwind

part, while it slightly overestimates them in the downwind part. At such a low wind velocity, blade/wake interactions are strong: the wake is slowly convected away due to the low wind velocity, and thus the downwind blades are strongly affected. The poor performance of the MSM model was expected, as no distinctions are made between the upwind and downwind parts. Once the stall models are activated (Figure 4, bottom), discrepancies arise on the upwind part for the tangential force coefficient: considering the BL/AC flow model, the stall model tends to lower down the values, while it has a negligible impact on the $\text{Oye}/V2D$, $\text{Oye}/V3D$ and Oye/MSM results. The induction from the AC model is based on the quasi steady forces. The 2D shed vorticity effects, which are part of the BL stall model, are applied afterwards to compute the unsteady forces. Because the shed vorticity is also responsible for the wake induction of a VAWT, it might be accounted for differently. Further, the time constants are chosen to the small dynamic stall loops typically found on HAWTs.

2.4. Low TSR, stalled flow

At lower TSR number no major differences occur between the four solvers when the stall models are deactivated (Figure 5, top). Both normal and tangential force coefficient evolutions are similar. Inductions are low, and the MSM model performs well. When stall models are activated

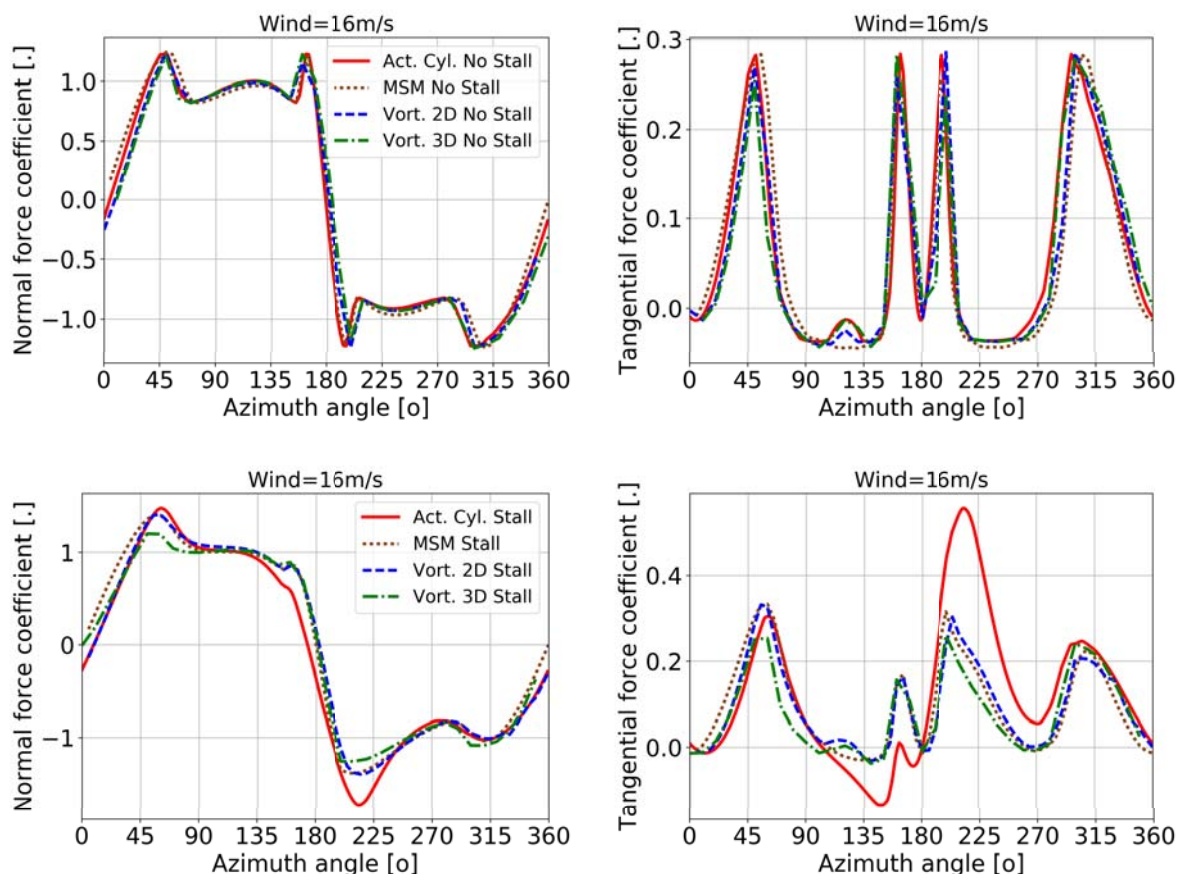


Figure 5. Normal (left) and tangential (right) force coefficients as a function of azimuthal position predicted by the AC model, the MSM model, the 2D and 3D vortex solvers without dynamic stall (top) and with dynamic stall (bottom) at $\text{TSR}=1.92$.

(Figure 5, bottom), differences appear (attack angles above the static stall are reached). Largest differences occur in the downwind part of the rotor. The predicted tangential force coefficient is much larger with the BL/AC flow model than with the Øye/MSM/vortex models. Regarding the normal force coefficient, results are consistent in the upwind part. The 3D vortex model predicts a weaker increase of the normal force near azimuth 45° compared to other solvers. In the downwind part, the BL/AC model deviate from the other models near azimuth 200° : a larger decrease of the normal force coefficient is predicted. Results of the MSM model are consistent with the other models: wake effects are weaker compared to the high TSR case, and stall dominates.

These observations can be related to the impact of the stall model, more visible in Figure 6. The normal and tangential force coefficients are given as a function of the geometrical angle of attack: this angle is based on purely geometrical considerations and can be used as a reference for all the models. Regarding the normal force coefficient evolution, the 3D vortex model predicts weaker hysteresis loops than the others at extreme attack angles (between -30° up to -10° and between 10° up to 30° , while the BL/AC model predicts much larger hysteresis. In the upwind part (positive angle of attack), prediction of the BL/AC model deviates quite largely from the other ones. A large influence of the attached flow module is visible (angles between 0° up to 15°).

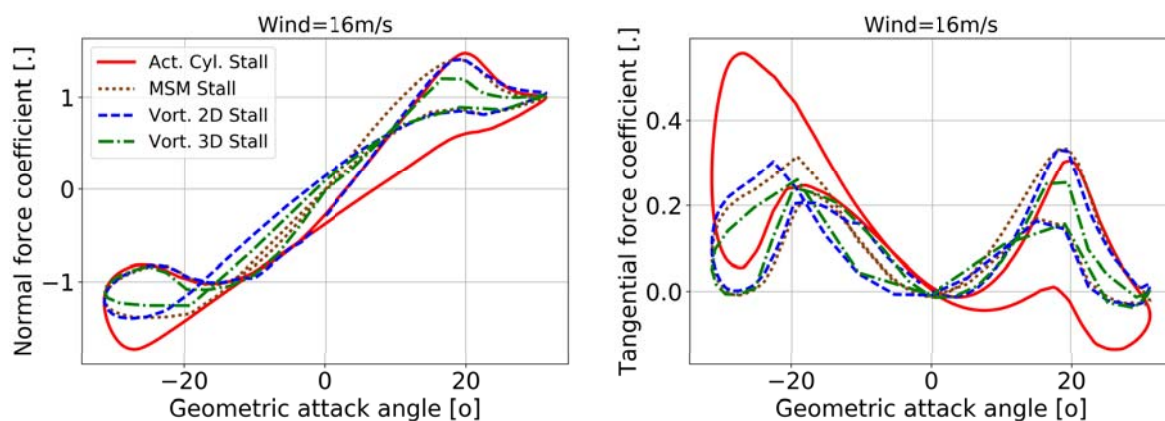


Figure 6. Normal (left) and tangential (right) force coefficients as a function of the geometrical angle of attack predicted by the 2D AC model, the MSM model, the 2D and 3D vortex solvers at $TSR=1.92$.

Regarding the tangential force coefficient, observations are similar. At positive angles of attack, hystereses are similar, and attached flow effects are much pronounced with the BL/AC flow model. At negative, high attack angles, the BL/AC model predicts higher tangential force coefficients, while the shape of the hysteresis is similar to the other solvers.

2.5. Conclusions

Based on the observations made above, it can be stated that both AC and V2D/V3D solvers lead to consistent results at low and high TSR values. The MSM model is consistent at low TSR, but fails at high TSR values. Some differences are noticed in the stall models. DTU implementation being based on a BL type model, while IFPEN solvers use the Øye model.

3. Fully-coupled, aero-elastic simulations of NENUPHAR's prototype

Aerodynamic models have been presented and compared in section 2. They will now be applied to the aero-elastic simulation of the NENUPHAR's 1HS onshore prototype. Both blades and struts are supposed to be flexible. We will focus on the comparison of the predicted and measured bending moments on the blades. First of all, the two aero-elastic solvers used in this study will be briefly introduced.

3.1. Presentation of the aero-elastic solver

3.1.1. DeepLines WindTM. DeepLines WindTM (Le Cunff et. al, [11] and [12]) is an aero-hydro-servo-elastic solver, capable of simulating complete floating wind turbine systems, including horizontal and vertical axis wind turbines. Structural components are modelled using non-linear beam finite elements, while hydrodynamic loads are based on linear and non-linear models (i.e. Morison elements, potential flow theory or quadratic transfer functions). Rotor control can be achieved by plugging in external dynamic libraries. The same procedure is used for the aerodynamic models: an external library is coupled with the solver. This library includes all of the IFPEN aerodynamic models mentioned previously. An implicit Newmark scheme is used for time integration.

3.1.2. HAWC2. The HAWC2 code is a code intended for calculating wind turbine response in time domain. The structural part of the code is based on a multibody formulation where each body is an assembly of Timoshenko beam elements. The turbine is modeled by an assembly of bodies connected with constraint equations, where a constraint could be a rigid coupling, a bearing, a prescribed fixed bearing angle etc. VAWT simulating feasibility has been added with the Actuator Cylinder approach, see the description of the implementation given in [15]. Analysis of VAWT aerodynamics and design using the Actuator Cylinder flow model have also been performed (Madsen et al., [14]). Control of the turbine is performed through one or more DLL's (Dynamic Link Library). The format for these DLL's is also very general, which means that any possible output sensor normally used for data file output can also be used as a sensor to the DLL. An example of the simulation capacity is described in the work of Larsen et al. [10].

3.2. Validation of the elastic models

A modal analysis has been first performed with the aero-elastic models: the results are compared with both the measured data and results from a 3D finite element model (Figure 7). The

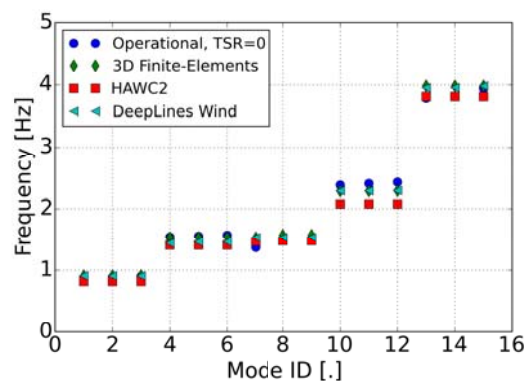


Figure 7. Modal analysis of the NENUPHAR's 1HS wind turbine.

first 12 modes correspond to strut modes, and modes 13 to 15 correspond to the first blade modes. Agreement between DeepLines WindTM and reference data is satisfactory, despite a slight underestimation of the frequencies for modes 4 to 9 (the relative error is between 2.5 and 5% compared with the 3D finite element solution, while it is below 1% for the other modes. Using HAWC2, frequencies are globally under-estimated, and especially modes 10 to 12. The relative error is in-between 4% and 9.2% for the whole set of modes. This may have an impact on the bending moments.

3.3. Results

The aero-elastic solver predictions, compared to the NENUPHAR's load measurements (strain gages *SG217* and *SG218* with respect to Figure 1 conventions), are shown in Figure 9. For the sake of clarity and readability, only the variations of the bending moment around a zeroed mean value are compared. Results including the mean value are given in Appendix A. Differences on the mean value are of limited interest in this paper since they can be attributed to mechanical effects (differences in mass, structural model, rotational speed) rather than aerodynamic ones. Negative values of the bending moment variations indicates that the blade tends to bend inwardly, towards the rotor axis, while it tends to bend outwardly for positive values. Using the DeepLines WindTM solver, a time step of 0.05 sec is chosen, with a simulation time of 600 sec. Using HAWC2, a time step of 0.01 sec is chosen, with a simulation time of 800 sec, first 200 sec being excluded to discard the transients. For the vortex solvers, approximately 8 full rotor rotations are kept in the wake. Two TSR are considered (2.5 and 3.5), under an high atmospheric turbulence intensity (in the order of 17.5%).

In the upwind part (azimuth between 0° and 180°), an over-prediction of the bending moment variations is observed between azimuth 0° to 90° . This over-prediction is most-likely due to an exceeding stall: it can be correlated with the results based on the rigid turbine configuration, see Figure 5. Such an over-estimation of the stall when compared to on-field measurements under highly turbulent flow was already observed by Blondel and Cathelain [3], while focusing on the comparison between measured and simulated normal forces on the Sandia 17 m VAWT. A possible explanation here is the delay of the static stall of the airfoil due to the presence of a turbulent inflow, as experimentally shown by Devinant et al. [4]. Using the 3D vortex solver (V3D), the stall effect is less pronounced (as already shown Figure 5), and the agreement with experimental data is better. This is due to the representation of the shed vorticity, which is different between the 2D and the 3D solver.

In the downwind part (azimuth 180° to 360°), the experimental trends are more or less followed. On the lower part of the blade, the impact of the tower is visible on the measured data, near azimuth 235° : a diminution of the bending moment is observed. While the BL/AC and \emptyset ye/V2D model tends to over-predict this phenomenon, the \emptyset ye/V3D and \emptyset ye/MSM models under-predict the tower impact. In the downwind part, the \emptyset ye/MSM model tends to over-predict the bending moment variations, especially in the lower blade part, where the local TSR is high. This is consistent with the observation made on the rigid turbine case: the MSM model, coupled with a dynamic stall model, performs better at low TSR, when the stall dominates. Similarly to the upwind part, the use of a three-dimensional solver (V3D) improves the results. Globally, in the upper blade part at TSR 3.5, all the solvers tend to over-estimate the variations of the bending moment in the downwind part. At TSR 2.5 and also in the lower blade part, the agreement is slightly better. These discrepancies are not explained yet, and further investigations are needed. In the upwind part, at TSR 2.5, the over-estimation, which is attributed to an exceed in stall, is located between azimuth 0° and 45° , while at TSR 3.5, the over-estimation covers the whole upwind part, up to an azimuth of 180° .

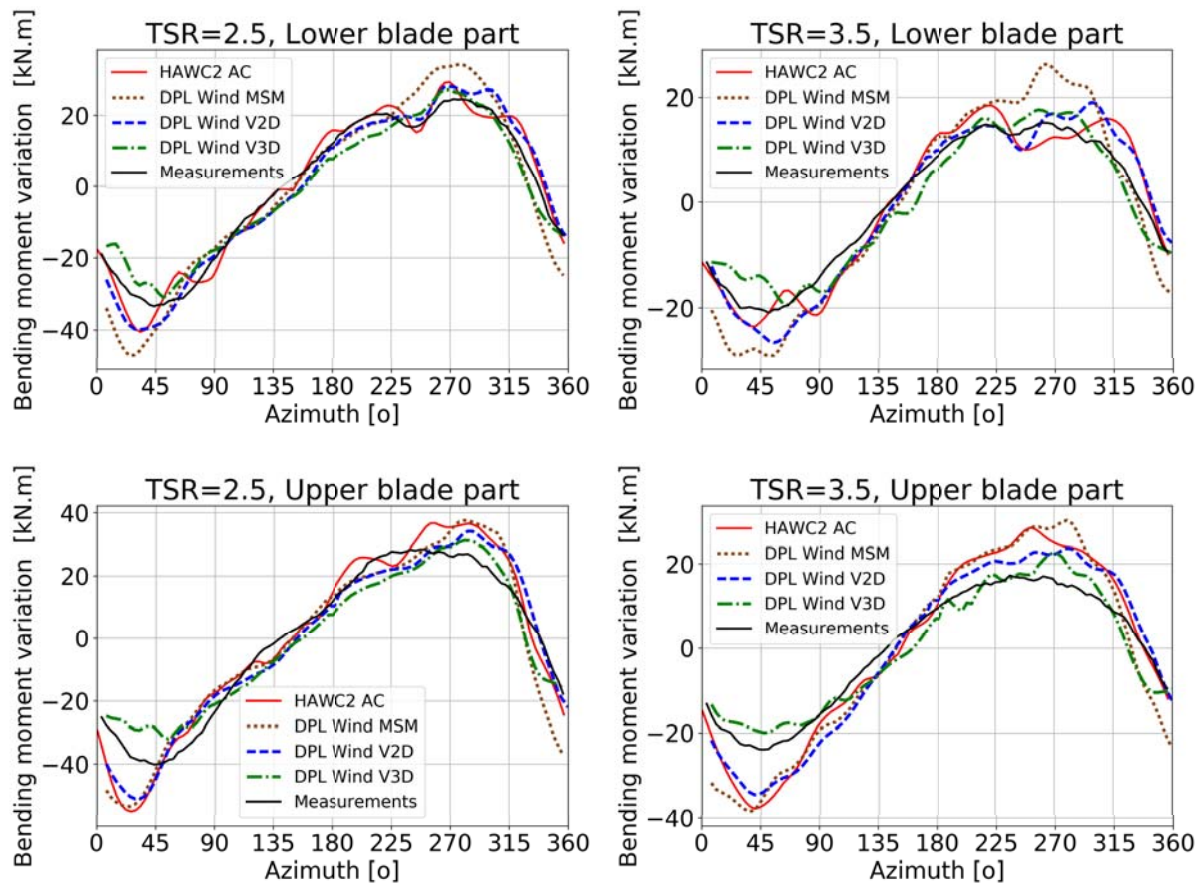


Figure 8. Variations of the bending moments around its mean value, lower part of the blade (top) and upper part of the blade (bottom), comparison between measurements, DeepLines WindTM and HAWC2 models, TSR=2.50 (left) and 3.50 (right).

3.4. Conclusions

Agreement between the solvers and measurements is acceptable. Even so some tendencies have been observed, further investigations are needed: other TSR should be considered. However, from the two TSR considered here, it can be concluded that all the models succeeded in predicting the variations of DPL of the bending moment of the blade in both lower and upper part.

4. Conclusions

In this paper, various aerodynamic models have been compared, including dynamic stall models. At low TSR, where the impact of the blade/wake interactions are low, a simple MSM model compare well with the more advanced models, due to the dominating effect of the dynamic stall and the low inductions. At lower TSR, differences tend to appear. Predictions of the aerodynamic models, coupled with elastic solvers, have been compared to the NENUPHAR's 1HS measurements data. A good agreement has been obtained. Some trends were noticed: an over-prediction of the bending moments was observed in the upwind part, and is attributed to an excessive stall. This might be a consequence of the high ambient turbulence, which tend to delay the static stall. The use of a 3D vortex model improves the results. At higher TSR, a global over-estimation of the bending moment variations has been noticed. Further studies are

required to draw final conclusions on this study (higher TSR, various turbulence levels).

Acknowledgments

This work is a part of the results of Work Package 3 of the INFLOW project, which was supported by the European Union's Seventh Programme for research, technological development and demonstration under grant agreement No 296043.

References

- [1] F. Blondel, R. Boisard, M. Milekovic, G. Ferrer, C. Lienard, D. Teixeira, Validation and comparison of aerodynamic modelling approaches for wind turbines, *J. Phys.: Conf. Ser.* 753 022029, TORQUE, 2016.
- [2] F. Blondel, G. Ferrer, M. Cathelain, D. Teixeira, Improving a BEM Yaw Model Based on NewMexico Experimental Data and Vortex/CFD Simulations, *Congrs Franais de Mcanique*, Lille, 2017.
- [3] F. Blondel, M. Cathelain, Benchmarking activities (code to code comparison) on the rigid IHS 3-Bladed VAWT, IFPEN report Ref.17.0186, 2017.
- [4] Ph. Devinant, T. Laverne, J. Hureau, Experimental study of wind-turbine airfoil aerodynamics in high turbulence, *J. Wind Eng. Ind. Aerodyn.* 90, 2002.
- [5] T.D. Economon, F. Palacios, S.R. Copeland, T.W. Lukaczyk, J.J. Alonso. SU2: An Open-Source Suite for Multiphysics Simulation and Design", *AIAA Journal*, Vol. 54, No. 3, 2016.
- [6] C.S. Ferreira, H.A. Madsen, M. Barone, B. Roscher, P. Deglaire, I. Arduin, Comparison of Aerodynamic Models for Vertical Axis Wind Turbines, *J. Phys.: Conf. Ser.* 524 012125, TORQUE, 2016.
- [7] M.H. Hansen, M. Gaunaa, H.A. Madsen, A Beddoes-Leishman type Dynamic Stall Model in State-Space and Indicial Formulations, Denmark. Risoe-R; No. 1354(EN), 2004.
- [8] J.W. Larsen, S.R.K. Nielsen, S. Krenk, Dynamic Stall Model for Wind Turbine Airfoils, *J. of Fluids and Structures* 23 pp. 959-982, 2007.
- [9] T.J. Larsen, H.A. Madsen, On the Way to Reliable Aeroelastic Load Simulation on VAWT's, preprint, DTU, 2013.
- [10] T.J. Larsen, G. Larsen, H.A. Madsen, S.M. Petersen, Wake effects above rated wind speed. An overlooked contributor to high loads in wind farms, *EWEA*, 2015.
- [11] C. Le Cunff, J.M. Heurtier, L. Piriou, C. Berhault, T. Perdrizet, D. Teixeira, G. Ferrer, J.C. Gilloteaux, Fully Coupled Floating Wind Turbine Simulator Based on Nonlinear Finite Element Method: Part I - Methodology, *OMAE2013-10780*, 2013.
- [12] C. Le Cunff, J.M. Heurtier, L. Piriou, C. Berhault, T. Perdrizet, D. Teixeira, G. Ferrer, J.C. Gilloteaux, Fully Coupled Floating Wind Turbine Simulator Based on Nonlinear Finite Element Method: Part II - Validation Results, *OMAE2013-10785*, 2013.
- [13] H.A. Madsen, The Actuator Cylinder, A Flow Model for Vertical Axis Wind Turbine, Institute of Industrial Constructions and Energy Technology, Internal report, 1982.
- [14] H.A. Madsen, U.S. Paulsen, L. Vitae, Analysis of VAWT aerodynamics and design using the Actuator Cylinder flow model, *J. Phys.: Conf. Ser.* 555 012065, TORQUE, 2012.
- [15] H.A. Madsen, T.J. Larsen, U.S. Paulsen, L. Vita, Implementation of the Actuator Cylinder Flow Model in the HAWC2 code for Aeroelastic Simulations on Vertical Axis Wind Turbines, 51st AIAA Aerospace Sciences Meeting, 2013.
- [16] S. Øye, Dynamic stall simulated as a time lag of separation, 4th IEA Symposium on the Aerodynamics of Wind Turbines, 1991.
- [17] G.R. Pirrung, M. Gaunaa, Dynamic Stall Model Modifications to Improve the Modeling of Vertical Axis Wind Turbines, DTU Wind Energy Report, 2016.
- [18] D. Pitance, S. Horb, J. Kluczevska-Bordier, A. Immas, F. Silvert, Experimental Validation of Pharwen Code Using Data From Vertical-Axis Wind Turbines, *WindEurope PO.123*, 2016.
- [19] G. Venet, A. Immas, R. Fuchs, N. Parneix, F. Silvert, A. Masson, P. Deglaire, Development and numerical validation of an aero-servo-elastic code for floating vertical-axis wind turbines, *EUROMECH COLLOQUIUM* 583, 2016.

Appendix A

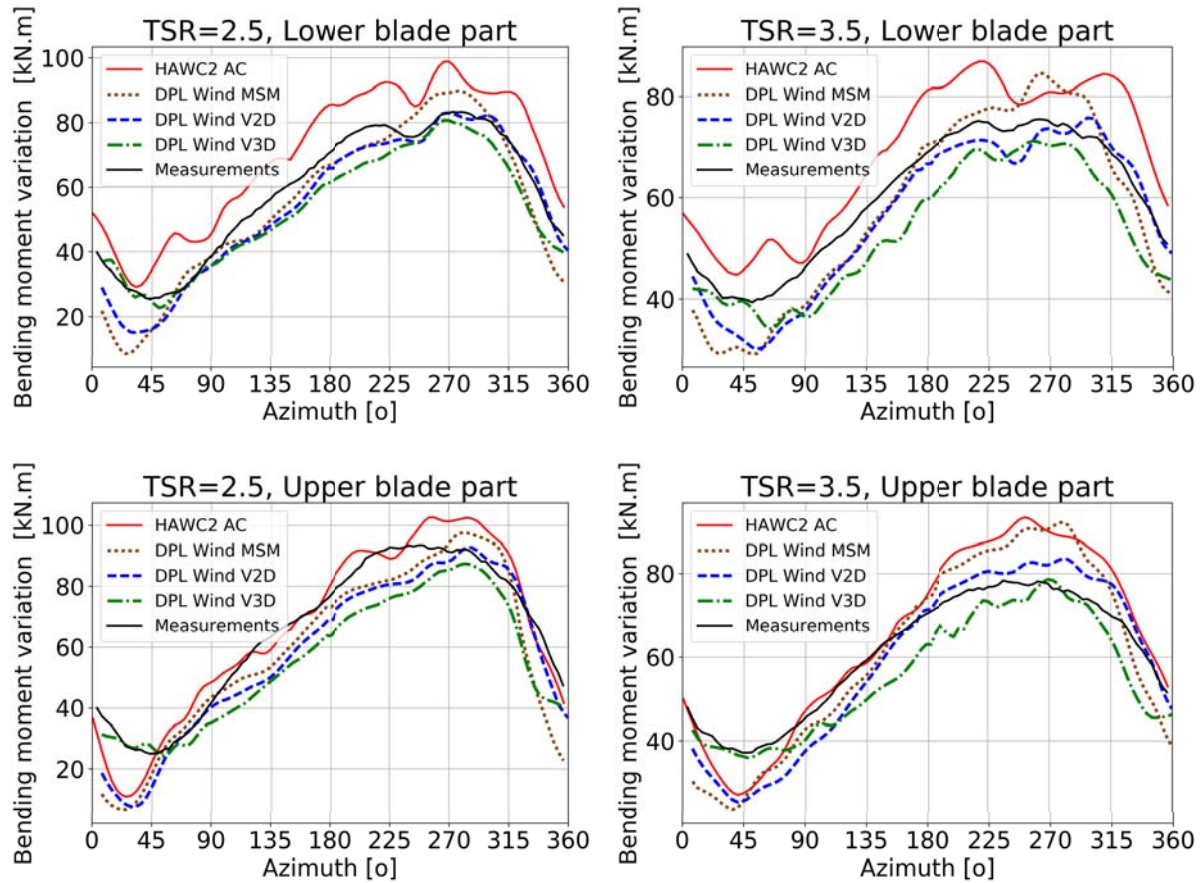


Figure 9. Absolute bending moments, lower part of the blade (top) and upper part of the blade (bottom), comparison between measurements, DeepLines WindTM and HAWC2 models, TSR=2.50 (left) and 3.50 (right).